Geosci. Model Dev. Discuss., 2, 1115–1155, 2009
www.geosci-model-dev-discuss.net/2/1115/2009/

Geoscientific Model Development Discussions

Geoscientific Model Development Discussions is the access reviewed discussion forum of *Geoscientific Model Development*

The efficient global primitive equation climate model SPEEDO

C. A. Severijns and W. Hazeleger

Royal Netherlands Meteorological Institute (KNMI), de Bilt, The Netherlands

Received: 10 August 2009 – Accepted: 14 August 2009 – Published: 26 August 2009

Correspondence to: C. A. Severijns (c.severijns@knmi.nl)

Published by Copernicus Publications on behalf of the European Geosciences Union.

Abstract

The efficient primitive-equation coupled atmosphere-ocean model SPEEDO is presented. The model includes an interactive sea-ice and land component. SPEEDO is a global earth system model of intermediate complexity. It has a horizontal resolution of T30 (triangular truncation at wave number 30) and 8 vertical layers in the atmosphere, and a horizontal resolution of 2 degrees and 20 levels in the ocean. The parameterizations in SPEEDO are developed in such a way that it is a fast model suitable for large ensembles or long runs on a workstation. The model has no flux correction. We compare the mean state and inter-annual variability of the model with observational fields of the atmosphere and ocean. In particular the atmospheric circulation, the mid-latitude patterns of variability and teleconnections from the tropics are well simulated. To show the model's capabilities, we performed a long control run and an ensemble experiment with enhanced greenhouse gasses. The long control run shows that the model is stable. CO_2 doubling and future climate change scenario experiments show a climate sensitivity of $1.84\,\mathrm{K\,W^{-1}\,m^{-2}}$, which is within the range of state-of-the-art climate models. The spatial response patterns are comparable to state-of-the-art, higher resolution models. However, for very high greenhouse concentrations the parameterizations are not valid. We conclude that the model is suitable for past, current and future climate simulations and for exploring wide parameter ranges and mechanisms of variability. However, as with any model, users should be careful when using the model beyond the range of physical realism of the parameterizations and model setup.

GMDD

2, 1115–1155, 2009

Efficient primitive equation climate model SPEEDO

C. A. Severijns and W. Hazeleger

1 Introduction

Numerical models of the earth system can be used for understanding processes in the earth system, understanding past climate changes and predicting future changes. Global state-of-the-art earth system models are computationally expensive which limits their use to simulate long time scales, to make large ensembles or to cover wide parameter ranges. For these scientific purposes computationally efficient earth system models of intermediate complexity (EMICs) have been developed. To achieve this computational efficiency, many EMICs have limited spatial resolution and incorporate a limited number of physical processes. Nevertheless, EMICs have shown to be invaluable in modern climate research. For example, they have been used to explain low-frequency variability in the climate system, can cover wide value ranges in parameter space and have been used to extend climate projections for future climate (Claussen et al., 2002).

A host of EMICs are currently used in the literature, ranging from energy balance models with prescribed atmospheric dynamics to 3-dimensional atmosphere and ocean models with interactive physics and dynamics (e.g., Smith et al., 2008; Farneti and Vallis, 2009). Here we report on the new global SPEEDO model which can be regarded as the successor of the ECBILT-CLIO model (Opsteegh et al., 1998; Goosse and Fichefet, 1999). ECBILT is a quasi-geostrophic atmosphere model with only 3 layers and limited resolved or parameterized physics. It has been used extensively in climate studies, for instance as part of the LOVECLIM earth system model (e.g., Roche et al., 2007). One of the drawbacks of the ECBILT model is that the quasi-geostrophic approximation breaks down in the tropics. Also, the prescribed clouds and the adjustment in the fresh water flux limit the application of the model. Here we report on the SPEEDO (Speedy-Ocean) model that has a primitive equation dynamical core in the atmosphere and fully interactive physics. Therefore, it does not have the limitations of ECBILT. However, its parameterizations are simplified (Molteni, 2003) and the resolution is coarse to allow for long runs.

GMDD
2, 1115–1155, 2009

The atmospheric model used in SPEEDO forced by observed surface conditions and coupled to a global slab ocean model and to a basin-scale ocean model has been used in many studies already (e.g., Molteni, 2003; Hazeleger and Haarsma, 2005; Hazeleger et al., 2005; Bracco et al., 2005; Kucharski et al., 2006; Breugem et al., 2007). In this paper we describe the fully global SPEEDO model and present a number of integrations of pre-industrial climate, current climate and projected future climate changes in order to validate the model, to compare it with state-of-the-art climate models and to demonstrate potential applications.

2 Model description

The SPEEDO model consists of a global atmosphere model, a global ocean and sea-ice model and a simple land-surface model. The current version does not include biogeochemical modules. Both the atmosphere and ocean components are based on the primitive equations. The parameterizations are simplified and described by Molteni (2003), with some modifications as described by Hazeleger et al. (2005). The parameterization package has been specially designed to work in models with just a few vertical levels, and is based on the same physical principles adopted in the schemes of state-of-the art GCMs. The parameterized processes include large-scale condensation, convection, clouds, short wave and long wave radiation, surface fluxes and vertical diffusion. We refer to the papers mentioned above for details on the numerics and parameterizations. The spectral triangular truncation is at total wave number 30 (T30) and there are 8 layers in the vertical. The advection scheme used in the original Speedy model does not conserve energy, tracers and dry air mass. In a coupled model these losses can result in a climate drift. Therefore a correction was added to the advection scheme of SPEEDO that compensates the loss of tracers and dry air mass. Furthermore, the model was tuned such that the energy loss only affects the energy budget at the top of the atmosphere. This ensures that the surface energy budget is closed and prevents drift in the ocean and land models. For estimating the parameters

GMDD
2, 1115–1155, 2009

the method of Severijns and Hazeleger (2005) has been applied to the atmosphere model before coupling to the ocean.

The ocean model used in SPEEDO is the CLIO model. We refer to Goosse and Fichefet (1999) for details on the ocean model. The CLIO model has 20 layers, uses a z-vertical coordinate and has a horizontal resolution of about 200 km. The LIM sea ice model is incorporated in CLIO.

The land model consists of a bucket model with three soil layers and two snow layers. It includes a simplified hydrology in which the run off is drained into the ocean at specific locations of major river outflows. The freezing and melting of soil moisture is taken into account. Each bucket has a fixed maximum soil moisture capacity. The land surface albedo is prescribed using a monthly climatology.

The atmosphere, land, and ocean/sea-ice components of SPEEDO exchange data via a coupler. The coupler is implemented as a library that is linked to each component model. This ensures that the coupling workload is evenly distributed between the CPUs and that the coupler's performance scales well. The atmosphere and land models use the same Gaussian latitude-longitude grid. The ocean and sea-ice model uses a curvilinear grid that is designed to prevent the pole problem. A first order conservative method is used to regrid data between the grids of the atmosphere and ocean models. Run off is collected in the land model in river basins and is transferred to the ocean model grid points close to major river outlets where it is distributed over the ocean. The coupled model runs without any flux correction.

Although the resolution of the SPEEDO model is relatively coarse, we will show that it is sufficient to resolve the main phenomena of the general circulation in the atmosphere and ocean. The model is sufficiently fast to perform century long runs on desktop computers. For example, it takes less than 20 min to simulate one year on an Intel Core 2 Duo E6850 CPU at 3 GHz. All runs discussed in this paper have been obtained from runs performed on a single workstation.

GMDD

2, 1115–1155, 2009

3 Results

Several simulations were performed with the SPEEDO model to compare it with observed climate data and results from state-of-the-art climate models. The model was spun up for a period of 2000 years under pre-industrial conditions. The final state of this spin up run was used as the initial condition in the year 1800 for the experiments presented in this paper. First, a 1000 year control run was done also under pre-industrial conditions to assess the stability of the model. Second, a five member ensemble of 300 year long experiments with perturbed initial condition was done with 19th and 20th century conditions and a scenario for the 21st century. The results of this ensemble are compared to observed climate data and CMIP3 model results (Meehl et al., 2007). Hereafter, a 200 year CO_2 doubling experiment was done to determine the climate sensitivity of SPEEDO. Finally, a 1200 year scenario experiment was done with an enhanced prescribed CO_2 concentration to determine the models transient climate response. In the following sections we present the results of these experiments.

3.1 Control simulation

To verify that the model is in equilibrium after the spin up, we performed a 1000 year long control simulation in which the equivalent CO_2 concentration was set to 261 parts per million (ppm) and the solar forcing was kept constant. We focus on the energy budget and the total heat and fresh water content in the ocean. In the case of a climate in equilibrium these should be constant. The global mean value, standard deviation and drift – the mean over the last 100 years minus the mean over the first 100 years – was computed for the following annual mean quantities: the top-of-the-atmosphere (TOA) energy budget, the surface energy budget, the two meter air temperature (T_{2m}), the ocean heat content and salinity and the sea ice volume. The results are shown in Table 1. For all quantities the drift is smaller than the standard deviation. The difference between the TOA and surface energy budgets is caused by the energy loss of $1.5\,\mathrm{W\,m^{-2}}$ in the atmosphere model. The net surface energy budget is positive

GMDD
2, 1115–1155, 2009

instead of zero because the latent heat difference between snow and rain is not taken into account in the model. As a result, the heat that is extracted from the land surface to melt snow is not compensated by a latent heat difference when snow instead of rain falls on the land surface. The energy budget of the model is closed because this latent heat is released in the atmosphere when snow is formed. The lack of drift in the T_{2m} shows that the underlying land and ocean/sea-ice models are in equilibrium and no flux correction is needed. The small changes in the ocean temperature and salinity show that ocean model is in equilibrium too. Note that the salinity in the ocean is not constant because CLIO is a constant volume ocean model. The data on the total sea ice volume shows that the sea ice model is also in equilibrium.

3.2 20th and 21st century ensemble simulations

3.2.1 Mean state

In order to compare SPEEDO with 20th century climate data (using primarily atmospheric reanalysis data; Kalnay et al., 1996) and data from CMIP3 models, a five member ensemble with perturbed initial condition was run for the period 1800 to 2100. The initial condition of each member was perturbed by adding a Gaussian noise term with a standard deviation of 0.1 K to the air temperature. The CO_2 concentration follows the observed historical CO_2 concentration from 1800 to 2000. From 2000 until 2100 it follows approximately the SRES A2 scenario (Nakicenovic et al., 2000). These CO_2 concentrations are obtained from the UVIC model (Montenegro et al., 2007) which contains a carbon cycle such that slight deviations from the A2 scenario occur. The model's climatology and budgets were computed for the time period from 1960 to 2000 in order to validate the 20th century model climate.

The global mean TOA and surface radiation and heat fluxes and budgets in the ensemble mean are compared to data from Kiehl and Trenberth (1997) and Trenberth et al. (2009) in Table 2. Both the TOA short and long wave radiation fluxes in SPEEDO are lower than in estimates from observations. This implies that the planetary albedo in

GMDD
2, 1115–1155, 2009

SPEEDO is higher than implied by observations. This is compensated by an increased trapping of long wave radiation. The surface short wave radiation flux is high and in combination with the low TOA short wave radiation budget we conclude that the absorption of short wave radiation by the atmosphere in the model is too low. Most of the excess surface short wave radiation is compensated by the surface long wave radiation. The surface latent heat flux in SPEEDO is in good agreement with the data. The sensible heat flux is in agreement with the 1997 data but higher than the 2009 data. After correcting the TOA and surface budgets for the heat loss in the atmosphere and the net surface heat flux as diagnosed in the control run, both budgets are very close to the values given by Trenberth et al. (2009).

To illustrate the general atmospheric circulation in SPEEDO we show the ensemble mean of the zonal wind at 925 hPa in SPEEDO in Fig. 1. The spatial structure of the zonal wind field resembles the reanalysis data fairly well. The southern storm track in SPEEDO is too weak and its maximum strength is located too far to the north. The Indian monsoon occurs at the correct location in the model but its maximum wind speed is too low.

As a further illustration, the zonal eddy component at 500 hPa is shown in Fig. 2 for December to February (DJF) and June to August (JJA). In DJF, when the atmospheric dynamics dominate the circulation characteristics, the zonal eddy component of SPEEDO shows the same spatial structure as the reanalysis data but the extreme values are too low. In JJA the resemblance is not as good but in this period the zonal eddy component is weak and local feedbacks tend to affect the circulation. It is noteworthy that these circulation components are comparable and in many aspects improved compared to an earlier atmosphere only version of the model (Molteni, 2003).

Figure 3 compares the cloud cover in SPEEDO with data from ISCCP (Rossow and Schiffer, 1991). The cloud cover over sea ice and land is generally in good agreement with the data. Over sea this is not the case. The cloud cover is too low in the Tropics and the storm track areas and there are too many clouds in the subsidence areas in the northern Tropical Pacific and the North and South Atlantic. A part of the cloud cover

GMDD
2, 1115–1155, 2009

problems in the Tropics is due to the fact that the cloud cover is diagnosed from the precipitation. However, these biases do not strongly affect the surface energy budget, as shown in the previous section.

The precipitation in SPEEDO is shown in Fig. 4. The cold tongue in the sea surface temperature (SST) along the equator in the Pacific causes a double Intertropical Convergence Zone in the boreal winter and at the same time causes the errors in the tropical cloud cover. The figure also shows that the model has too much precipitation in tropical Africa and the Amazon and too little rain over tropical Atlantic and the warm pool. These are typical features of coarse resolution climate models.

SPEEDO is a coupled atmosphere-ocean model and the ocean can evolve freely. The difference of the SST in SPEEDO and observations (Stephens et al., 2001) is shown in the left panel of Fig. 5. The temperatures in the Tropics, in the Arctic and near Antarctica are slightly too high. The boundary current areas and the subtropical stratocumulus areas near the coast are also too warm. In the remaining area the temperatures are too low, especially in the South Atlantic. These biases are within the spread of the CMIP3 multi-model ensemble.

For the ocean, the meridional overturning circulation is important as it transports heat, fresh water and tracers within the earth system. The 41 year mean Atlantic meridional overturning circulation (AMOC) is shown in the right panel of Fig. 5. The upper cell is slightly stronger than $8\times10^6\,m^3\,s^{-1}$. This is approximately $3\times10^6\,m^3\,s^{-1}$ weaker than under pre-industrial conditions in the control run and about $8\times10^6\,m^3\,s^{-1}$ too weak compared to estimates of e.g. Cunningham et al. (2007), probably associated with low production of North Atlantic Deep Water. The strength of the Antarctic Bottom Cell is good for a coarse resolution model. The time mean global and Atlantic heat transport of all ensemble members are shown in Fig. 6. Inferences of observations of this quantity depends on inverse modeling. Also, surface fluxes from atmospheric reanalysis can be used. Compared to values derived from reanalysis (Kalnay et al., 1996), the Atlantic heat transport is too low as can be expected from the weak AMOC. The global heat transport in the Northern Hemisphere is also small but in the Southern

GMDD
2, 1115–1155, 2009

Hemisphere seems good. The model's internal variability causes the heat transport to vary by 0.05 PW.

The monthly ensemble mean sea ice cover in the Arctic and Antarctic for March and September is compared to the sea ice cover data from Cosimo (2008) in Figs. 7 and 8 respectively. It is evident that in both hemispheres the sea ice cover at the end of the summer is too low. The winter sea ice cover is slightly too large. The reason for this large seasonal cycle in the sea ice cover is unknown.

3.2.2 Variability

The main patterns of inter-annual variability in the Northern Hemisphere are the Pacific North American (PNA) and the North Atlantic Oscillation (NAO) patterns. The correlations of the PNA index with the Z500 anomalies and of the NAO index with the mean sea-level pressure (MSLP) anomalies are shown Fig. 9. The NAO index is computed here as the difference of the MSLP anomalies in the area 70° W to 10° W and 55° N to 77° N and the area 70° W to 10° W and 35° N to 45° N. The anomalies are with respect to the ensemble mean in order to suppress the global warming signal. The correlation was computed for the data of all ensemble members. The PNA pattern displays a well-known wave train, indicating that the response to tropical convection is good. The NAO pattern shows the familiar dipole pattern. The pattern is slightly shifted to the west compared to observations. Because of the coarse resolution of the ocean model we do not show the El Niño Southern Oscillation (ENSO). Variability does occur in the tropical Pacific, but it is far too weak compared to observations. For example, the standard deviation of the monthly mean NINO34 index is 0.23 K and the power spectrum of the NINO34 index has no peak at the time scales corresponding to the ENSO phenomenon.

At multidecadal time scales, an interhemispheric dipole pattern is found in observations in the Atlantic: the Atlantic Multidecadal Oscillation (AMO). The pattern of the AMO is shown in the upper panel of Fig. 10. The pattern was computed using the SST anomalies of individual members with respect to the ensemble mean SST in order to

GMDD
2, 1115–1155, 2009

remove the global mean trend in the SST. We regressed the SST anomalies onto an AMO index that is defined as the mean SST anomaly from 25° N to 60° N and 75° W to 7° W. Only statistically significant data with r^2>0.1 is shown. It can be seen in the lower panel of Fig. 10 that the AMO index has a red noise spectrum. Unlike some other models (Knight et al., 2005), the AMO index is only weakly correlated to the anomalies in the AMOC with a maximum correlation of about 0.5.

At centennial time scales, dominant ocean variability is found in SPEEDO. We analyzed the data from the 1000 year control run because the oscillations remain present during the complete control run while in the ensemble they disappear when the sea ice melts due to global warming. The time series of the maximum strength of the AMOC and its power spectrum are shown in Fig. 11. An AR(1) spectral analysis of the AMOC time series shows that the AMOC has a red noise spectrum (with more than 95% confidence).

The total sea ice volume in the Arctic (see Fig. 12) varies slightly on centennial time scales. The Antarctic sea ice volume varies much more on this time scale. The power spectrum of the annual mean Antarctic sea ice volume has a large broad peak at time scales of 100 to 250 years (see Fig. 13). An AR(1) spectral analysis shows that this peak is significant with more than 95% confidence in both hemispheres.

The regression of the Antarctic sea ice volume with the strength of the global meridional overturning circulation is shown in Fig. 14. This regression suggests that the oscillations in the sea ice volume are caused by a local interaction of the sea ice with the ocean. This is confirmed by regressions of the Antarctic sea ice volume with the sea water temperature at various levels in the ocean model (not shown). The regression of the sea ice volume with the AMOC is nowhere statistically significant. The mechanism of this variability is associated with interaction between sea ice, ocean convection, and vertical mixing. In short, while ice volume grows, heat is stored in the deeper layers. This heat is released when the water column becomes unstable and causes the sea ice to retreat. A detailed analysis of this variability is beyond the scope of this paper.

Finally, we show the long-term trend in SPEEDO, forced by the growing greenhouse

gas concentrations in the 20th century. The global mean two meter air temperature in the SPEEDO ensemble is compared to those from some CMIP3 models for the period 2000 to 2100 (Fig. 15). We did not include information on aerosols in the model. SPEEDO tends to be colder and warms slightly faster compared to other models. However, the model follows the observed warming in the mid-20th century, the reduced warming afterward and steep warming from the late 20th century on.

3.3 CO_2 doubling experiment

In order to study the model's climate sensitivity a CO_2 doubling simulation was performed. In this experiment the model was restarted from the same conditions as the control experiment at a CO_2 concentration of 261 ppm and was run for 200 years with a CO_2 concentration of 522 ppm. The model reached quasi-equilibrium after 100 years. The spatial patterns shown in this section are the differences between the climatologies computed from the second 100 years of the CO_2 doubling run and the control run. Our results are compared to the responses of state-of-the-art climate model integrations collected by CMIP3 (Meehl et al., 2007).

The mean TOA radiation budget in the CO_2 doubling experiment is 1.74 $W\,m^{-2}$ larger than in the control run. The increase in the global mean surface temperature of 3.20 K in SPEEDO agrees well with the equilibrium climate sensitivity of 2.7 to 4.4 K in CMIP3 models. The climate sensitivity of SPEEDO is thus 1.84 $K\,W^{-1}\,m^{-2}$.

The time series of global mean T_{2m} in Fig. 16 shows that the model is close to equilibrium after 200 years, although the deep ocean still warms. The spatial structure of the model's T_{2m} response is very similar to the CMIP3 models, with largest warming in the Arctic due to the reduction of the snow cover and the sea ice extent.

The differences of the zonal averaged air temperature and specific humidity are shown in Fig. 17. The response shows the well-known tropospheric warming and stratospheric cooling. The highest warming is found in the upper troposphere in the tropics and near the surface in the Arctic region. The increased greenhouse trapping causes the humidity to increase, with a maximum at the surface in the tropics, consis-

GMDD
2, 1115–1155, 2009

tent with the Clausius Clapeyron relation. These features are consistent with results from the CMIP3 models.

The AMOC weakens significantly under $2\times CO_2$ conditions as can be seen in Fig. 18. The maximum overturning strength reduces by $8\times10^6\,m^3\,s^{-1}$ during the first 75 years and after that remains stable at a value of about $3\times10^6\,m^3\,s^{-1}$. The weakening is primarily associated with a reduction of North Atlantic Deep Water production.

The differences in the sea ice cover in March and September for both hemispheres are shown in Fig. 19. The sea ice cover in the Arctic is lower than in the control run which is to be expected. However the sea ice cover in the Southern Ocean in September increases. A comparison of the time series of the Antarctic sea ice volume in both runs shows that the control runs has two heat release events between 1800 and 2000 while the $2\times CO_2$ run has none. As a result, the time mean sea ice cover in the control run is lower in the areas where the heat stored in the deep ocean is released (see previous section).

3.4 Application: transient climate response

Earth system models of intermediate complexity, such as SPEEDO, can be used to explore a wide parameter range or to study long-term variability. Here we demonstrate an application of a long term climate projection and a large perturbation in greenhouse gas concentrations. We performed a simulation of 1200 years with transient varying CO_2 concentrations (see Fig. 20). From 1800 to 2100 the same CO_2 concentrations are used as in the ensemble experiment. From the year 2100 onward the rate of increase of the CO_2 concentration decreases until a maximum concentration of 1967 ppm is reached in the year 2282. Hereafter, the CO_2 concentration decreases slowly due to uptake in the ocean and sedimentation of calcium carbonate. After the year 2000 an extra freshwater flux, F_G, was added to the runoff of Greenland to account for the melting of its land ice sheet. The melting rate of the ice sheet is prescribed as

$$F_G = a.\max(< T_{2m} > - < T_{2m,2000} >, 0) \quad (1)$$

GMDD
2, 1115–1155, 2009

where $<T_{2m}>$ is the ten year running mean of the annual global mean two meter temperature, $<T_{2m,2000}>$ is the value of this quantity in the year 2000, and the fresh water flux coefficient a=10^4 m^3 s^{-1} K^{-1} (Marsh et al., 2007).

The time series of the annual global mean T_{2m} is shown in Fig. 20. The model shows a large warming. At very high CO_2 concentrations, the model response is too strong. The T_{2m} increases by 16 K while one would expect an increase of 8 to 9 K based on the climate sensitivity determined in the 2×CO_2 experiment.

The time series of the annual global mean TOA and surface energy budgets in Fig. 21 show that the ocean/sea-ice model takes up heat during most of the period. The maximum heat uptake occurs in the first half of the 22nd century. This is roughly 150 years earlier than the maximum in the CO_2 concentration. At the end of the run, the TOA budget has returned to its initial value. However, the final value of the surface budget is about 0.5 W m^{-2} smaller than its starting value. This is in agreement with the slight increase of the global mean T_{2m} and suggests that the ocean is still taking up heat.

This experiment shows that the model can be used to make long simulations and explore wide parameter ranges. It also shows that there are limits to the use of the model. This is the main reason why we present this experiment in this paper. The model shows excessive heating at high CO_2 concentrations. There are a number of limitations associated with the parameterizations used in the model because they are simplified to make the model fast. One of the problems is that only the absorptivity parameter in the CO_2 band changes with the CO_2 concentration. For this experiment with high CO_2 levels, the bandwidth probably needs to be changed as well. Also, there is large dependence on the relative humidity profile in a number of parameterizations, which go beyond the range of application. It shows that when wide parameter ranges are explored, the model's physics should always be checked for physical realism.

GMDD
2, 1115–1155, 2009

4 Conclusions

The coupled model of intermediate complexity SPEEDO was presented in this paper. This model is fast due to its simplified physics parameterization and relatively coarse resolution. However, the model is a full 3-dimensional model of the atmosphere and ocean, using primitive equations and a realistic configuration of continents, orography and bathymetry. Important new features with respect to its predecessor ECBILT-CLIO are the use of primitive equations, the lack of flux correction and fully interactive clouds and radiation. Only land surface albedo (monthly climatology), maximum soil moisture capacity (fixed), solar forcing and atmospheric composition is prescribed. Earlier coupled SPEEDO versions contained only basin-scale ocean models and have been extensively used in climate variability studies. Here, we reported on a globally coupled SPEEDO model, without flux corrections.

The validation of the model shows that it performs well in recent climate setting. The mean state of the atmosphere, especially the stationary waves in the mid-latitudes are well simulated given the coarse resolution. Also, the mid-latitude inter-annual variability and the long-term trends forced by rising greenhouse gas concentrations compare well to observations and to CMIP3 models. The climate sensitivity is within the range of state-of-the-art models and the main features of spatial variability, such as Arctic amplification, reducing AMOC, tropospheric heating are well simulated.

The main biases are a too large seasonal cycle in sea ice cover, a double intertropical convergence zone and a cold mid-latitude surface ocean. In addition, the meridional overturning circulation in the Atlantic is rather weak and the centennial variability in the sea ice volume may not be realistic. However, these biases are within the range of the inter-model variations of state-of-the-art models of CMIP3.

So, despite the coarse resolution realistic climate features are simulated. Apparently, the major climate feedbacks are included in the model. This makes the model very suitable to study past, recent and projected future climates. In particular large ensembles or long runs can be easily done on a single workstation. There are caveats,

GMDD
2, 1115–1155, 2009

however. We deliberately showed that the model's sensitivity may be too high at high levels of greenhouse gasses. Also, this model does not include a dynamical ice-sheet model. These limitations should be beard in mind when using the model far out of the range of recent climate fluctuations. In addition, the coarse resolution inhibits the use of the model for very regionalized climate studies. Limitations of intermediate complexity model are inherent to the chosen strategy. We believe that this model can be very useful in the hierarchy of simple 1-dimensional models to highly complex 3-dimensional earth system models.

The source code of the SPEEDO model is available at:
http://www.knmi.nl/onderzk/CKO/SPEEDO.html.

Acknowledgements. We acknowledge the modeling groups, the Program for Climate Model Diagnosis and Intercomparison (PCMDI) and the WCRP's Working Group on Coupled Modeling (WGCM) for their roles in making available the WCRP CMIP3 multi-model dataset. Support of this dataset is provided by the Office of Science, US Department of Energy.

References

Bracco, A., Kucharski, F., Molteni, F., Hazeleger, W., and Severijns, C.: Internal and forced modes of variability in the Indian Ocean, Geophys. Res. Lett., 32, L12707, doi:10.1029/2005GL023154, 2005. 1118

Breugem, W. P., Hazeleger, W., and Haarsma, R. J.: Mechanisms of northern tropical Atlantic variability and response to CO_2 doubling, J. Climate, 20, 11, 2691–2705, 2007. 1118

Claussen, M., Mysak, L. A., Weaver, A. J., et al.: Earth system models of intermediate complexity: closing the gap in the spectrum of climate system models, Clim. Dynam., 18, 579–586, 2002. 1117

Cosimo, J.: Bootstrap sea ice concentrations from NIMBUS-7 SMMR and SSM/I, January 1978 to December 2007, Boulder, Colorado USA, National Snow and Ice Data Center, digital media, 1999, updated 2008. 1124, 1141

Cunningham, S. A., Kanzow, T., Rayner, D., Baringer, M. O., Johns, W. E., Marotzke, J., Longworth, H. R., Grant, E. M., Hirschi, J. J.-M., Beal, L. M., Meinen, C. S., and Bryden, H. L.: Temporal variability of the Atlantic Meridional Overturning Circulation at 26° N, Science, 317, 935–938, 2007. 1123

Farneti, R. and Vallis, G. K.: An Intermediate Complexity Climate Model (ICCMp1) based on the GFDL flexible modeling system, Geosci. Model Dev., 2, 73–88, 2009. 1117

Goose, H. and Fichefet, T.: Importance of ice-ocean interactions for the global ocean circulation: a model study, J. Geophys. Res., 104(C10), 23337–23355, 1999. 1117, 1119

Hazeleger, W., Severijns, C., Seager, R., and Molteni, F.: Tropical Pacific-driven decadal energy transport variability, J. Climate, 18, 2037–2051, 2005. 1118

Hazeleger, W. and Haarsma, R. J.: Sensitivity of tropical Atlantic climate to mixing in a coupled ocean-atmosphere model, Clim. Dynam., 25, 4, 387–399, 2005. 1118

Hazeleger, W., Severijns, C., Haarsma, R., Selten, F., and Sterl, A.: SPEEDO: model description and validation of a flexible coupled model for climate studies, Technical report 257, KNMI, De Bilt, The Netherlands, 38 pp., 2003.

Kalnay, E., Kanamitsua, M., Kistler, R., et al.: The NCEP/NCAR 40-year reanalysis project, B. Am. Meteorol. Soc., 77, 437–470, 1996. 1121, 1123, 1135, 1136

Kiehl, J. T. and Trenberth, K. E.: Earth's annual global mean energy budget, B. Am. Meteorol. Soc., 78, 197–208, 1997. 1121, 1134

Knight, J. R., Allan, R. J., Folland, C. K., et al.: A signature of persistent natural thermohaline circulation cycles in observed climate, Geophys. Res. Lett., 32, L20708, doi:10.1029/2005GL024233, 2005. 1125

Kucharski, F., Molteni, F., and Bracco, A.: Decadal interactions between the western tropical Pacific and the North Atlantic Oscillation, Clim. Dynam., 26, 79–91, 2006. 1118

Marsh, R., Hazeleger, W., Yool, A., and Rohling, E.: Stability of the thermohaline circulation under millennial CO_2 forcing and two alternative controls on Atlantic salinity, Geophys. Res. Lett., 34, L03605, doi:10.1029/2006GL027815, 2007. 1128

Meehl, G. A., Covey, C., Delworth, T., Latif, M., McAvaney, B., Mitchell, J. F. B., Stouffer, R. J., and Taylor, K. E.: The WCRP CMIP3 multi-model dataset: A new era in climate change research, B. Am. Meteorol. Soc., 88, 1383–1394, 2007. 1120, 1126

Molteni, F.: Atmospheric simulations using a GCM with simplified physical parameterizations. I: Model climatology and variability in multi-decadal experiments, Clim. Dynam., 20, 175–191, 2003. 1117, 1118, 1122

GMDD

2, 1115–1155, 2009

Montenegro, A., Brovkin, V., Eby, M., Archer, D., and Weaver, A. J.: Long term fate of anthropogenic carbon, Geophys. Res. Lett., 34, L19707, doi:10.1029/2007GL030905, 2007. 1121

Nakicenovic, N., Alcamo, J., Davis, G., et al.: Special Report on Emissions Scenarios: A Special Report of Working Group III of the Intergovernmental Panel on Climate Change, Cambridge University Press, Cambridge, UK, 599 pp., 2000. 1121

Opsteegh, J. D., Haarsma, R. J., Selten, F. M., and Kattenberg, A.: ECBILT: A dynamic alternative to mixed boundary conditions in ocean models, Tellus, 50A, 348–367, 1998. 1117

Roche, D. M., Dokken, T. M., Goosse, H., Renssen, H., and Weber, S. L.: Climate of the Last Glacial Maximum: sensitivity studies and model-data comparison with the LOVECLIM coupled model, Clim. Past, 3, 205–224, 2007, http://www.clim-past.net/3/205/2007/. 1117

Rossow, W. B. and Schiffer, R. A.: ISCCP Cloud Data Products, B. Am. Meteorol. Soc., 71, 2–20, 1991. 1122, 1137

Severijns, C. A. and Hazeleger, W.: Optimizing parameters in an atmospheric general circulation model, J. Climate, 18, 17, 3527–3535, 2005. 1119

Smith, R. S., Gregory, J. M., and Osprey, A.: A description of the FAMOUS (version XDBUA) climate model and control run, Geosci. Model Dev., 1, 53–68, 2008. 1117

Stephens, C., Antonov, J. I., Boyer, T. P., Conkright, M. E., Locarnini, R. A., O'Brien, T. D., and Garcia, H. E.: World Ocean Atlas 2001, Volume 1: Temperature, edited by: Levitus, S., NOAA Atlas NESDIS 49, US Government Printing Office, Wash., D.C., 167 pp., 2002. 1123, 1139

Trenberth, K. E., Fasullo, J. T. and Kiehl, J. T.: Earth's Global Energy Budget, B. Am. Meteorol. Soc., 90, 311–324, 2009. 1121, 1122, 1134

Xie, P. and Arkin, P. A.: Analysis of global monthly precipitation using gauge observations, satellite estimates, and numerical model predictions, J. Climate, 9, 840–858, 1996. 1138

Table 1. The time mean value, the standard deviation and the drift of the TOA and surface energy budgets, the global mean two meter temperature, the global mean ocean temperature and salinity and the total sea ice volume. The drift is defined in the text.

Quantity	Mean value	Standard deviation	Drift	Unit
TOA budget	2.491	$1.839\ 10^{-1}$	$1.052\ 10^{-2}$	$\mathrm{W\,m^{-2}}$
Surface budget	1.053	$1.841\ 10^{-1}$	$1.352\ 10^{-2}$	$\mathrm{W\,m^{-2}}$
T_{2m}	285.3	$2.526\ 10^{-1}$	$-6.342\ 10^{-2}$	K
Ocean temperature	277.3	$1.092\ 10^{-2}$	$-7.092\ 10^{-3}$	K
Salinity	34.70	$1.856\ 10^{-5}$	$1.144\ 10^{-5}$	PSU
Sea ice volume	15.37	1.436	1.018	$10^{12}\ \mathrm{m^3}$

GMDD
2, 1115–1155, 2009

Table 2. The ensemble mean global mean radiation and heat flux budgets at the top of the atmosphere and the surface in the SPEEDO model compared to the results published by Kiehl and Trenberth (1997) and Trenberth et al. (2009). Positive values indicate downward fluxes.

Flux or budget in W m^{-2}	SPEEDO	Kiehl and Trenberth (1997)	Trenberth et al. (2009)
TOA short wave radiation	227.3	235	239.4
TOA long wave radiation	−223.9	−235	−238.5
Surface short wave radiation	173.6	168	161.2
Surface long wave radiation	−69.0	−66	−63
Surface latent heat	−78.3	−78	−80.0
Surface sensible heat	−24.5	−24	−17
TOA budget	3.4	0	0.9
Surface budget	1.9	0	0.9

GMDD
2, 1115–1155, 2009

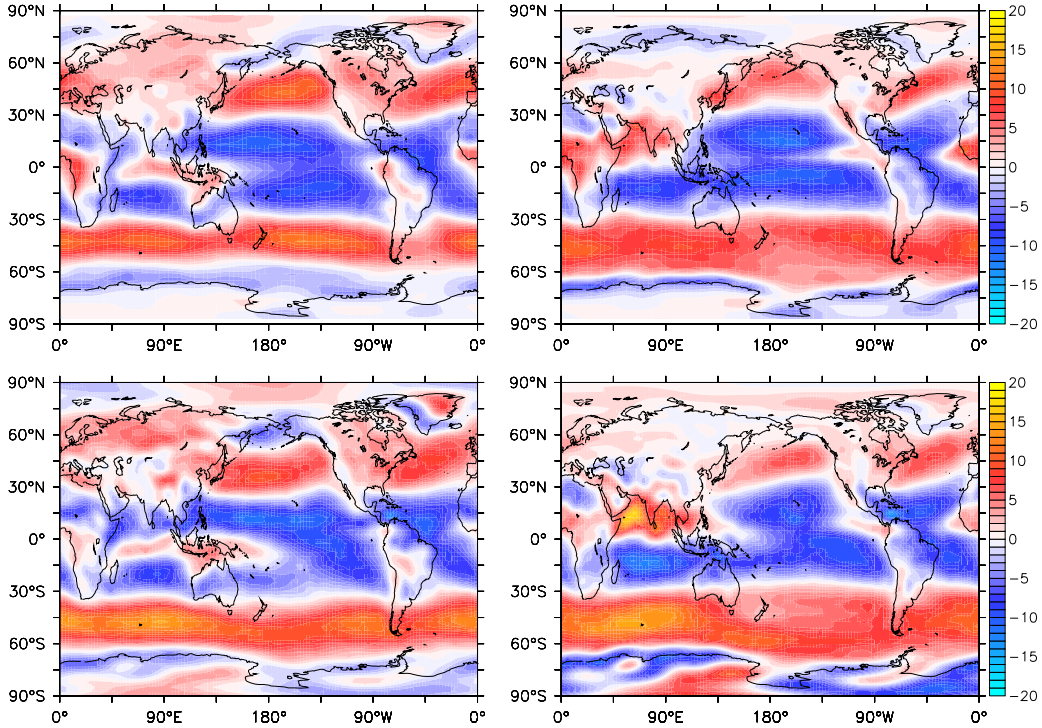

Fig. 1. The zonal wind at 925 hPa in $m\,s^{-1}$ in DJF (left) and JJA (right) of the mean of the SPEEDO ensemble (top) and the reanalysis data from Kalnay et al. (1996), (bottom).

GMDD

2, 1115–1155, 2009

Efficient primitive equation climate model SPEEDO

C. A. Severijns and W. Hazeleger

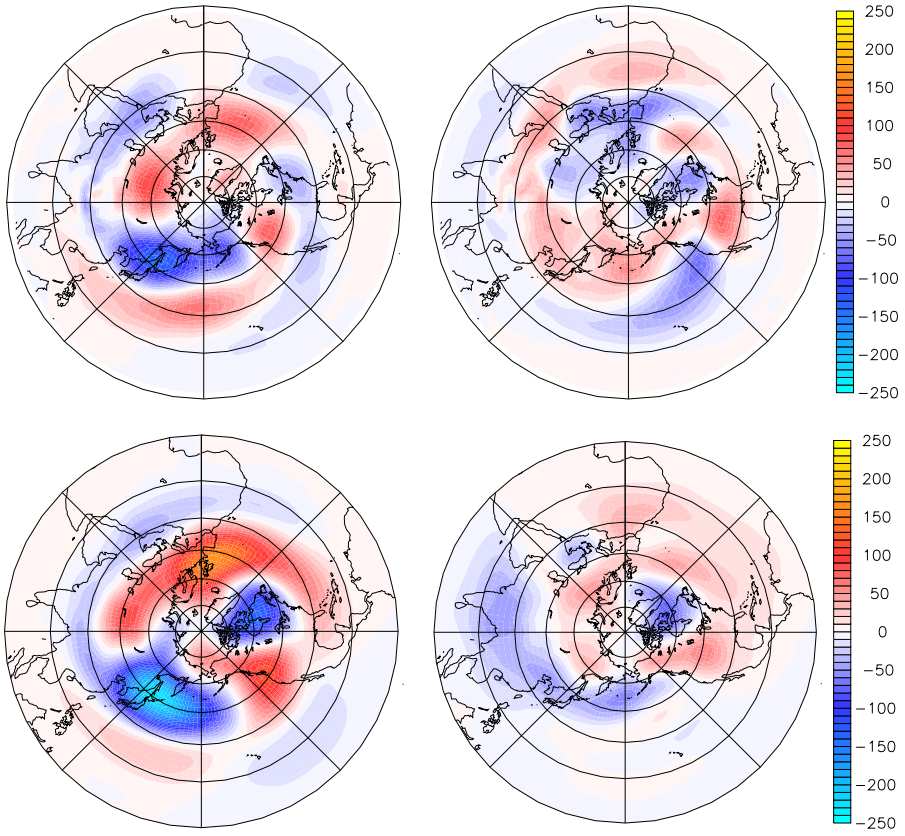

Fig. 2. The zonal eddy component of the geopotential height at 500 hPa in m in DJF (left) and JJA (right) of the mean of the SPEEDO ensemble (top) and the reanalysis data from Kalnay et al. (1996), (bottom).

GMDD
2, 1115–1155, 2009

Efficient primitive equation climate model SPEEDO

C. A. Severijns and W. Hazeleger

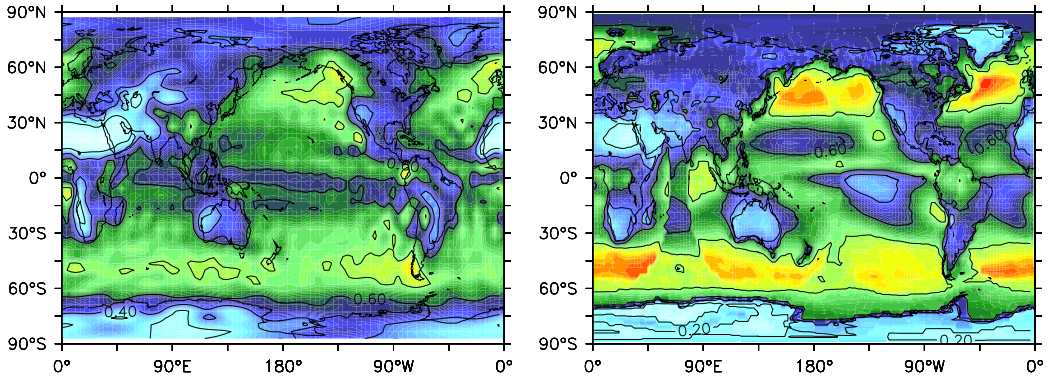

Fig. 3. The annual mean cloud cover fraction for the mean of the SPEEDO ensemble (left) and according to Rossow and Schiffer (1991), (right).

GMDD
2, 1115–1155, 2009

Efficient primitive equation climate model SPEEDO

C. A. Severijns and W. Hazeleger

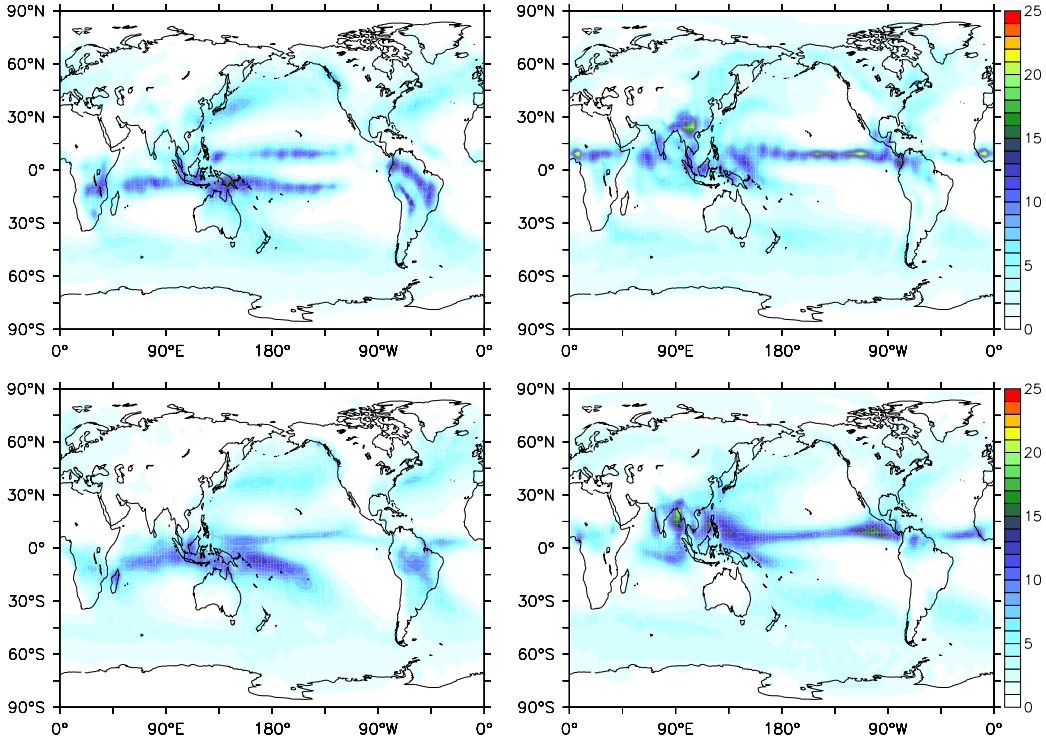

Fig. 4. The total precipitation in mm day^{-1} in DJF (left) and JJA (right) for the mean of the SPEEDO ensemble (top) and from Xie and Arkin (1996), (bottom).

GMDD
2, 1115–1155, 2009

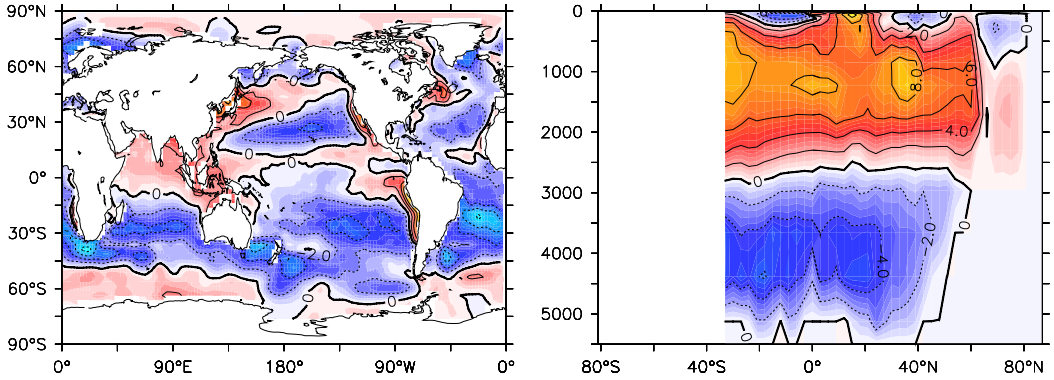

Fig. 5. The difference between the ensemble global mean SST in SPEEDO and the SST according to Stephens et al. (2001) in K (left) and the Atlantic meridional overturning circulation in 10^6 m^3 s^{-1} in SPEEDO (right).

GMDD

2, 1115–1155, 2009

Efficient primitive equation climate model SPEEDO

C. A. Severijns and W. Hazeleger

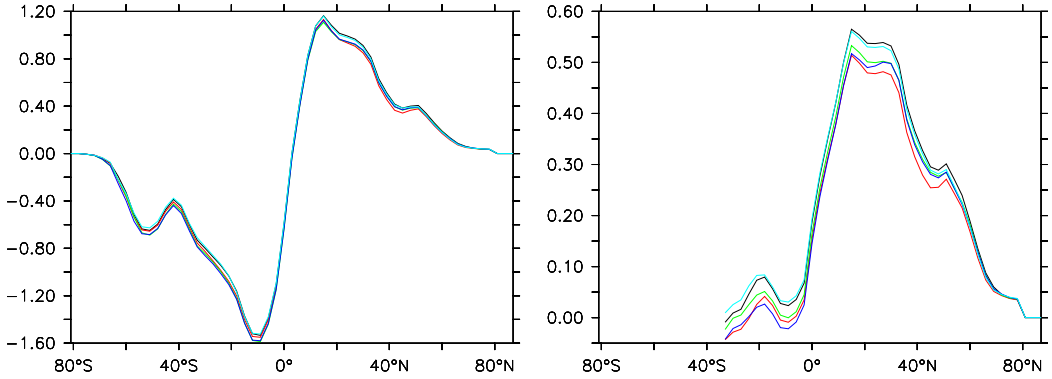

Fig. 6. The global (left) and Atlantic (right) ocean heat transport in PW for each member of the SPEEDO ensemble. Positive values indicate northward transport.

GMDD

2, 1115–1155, 2009

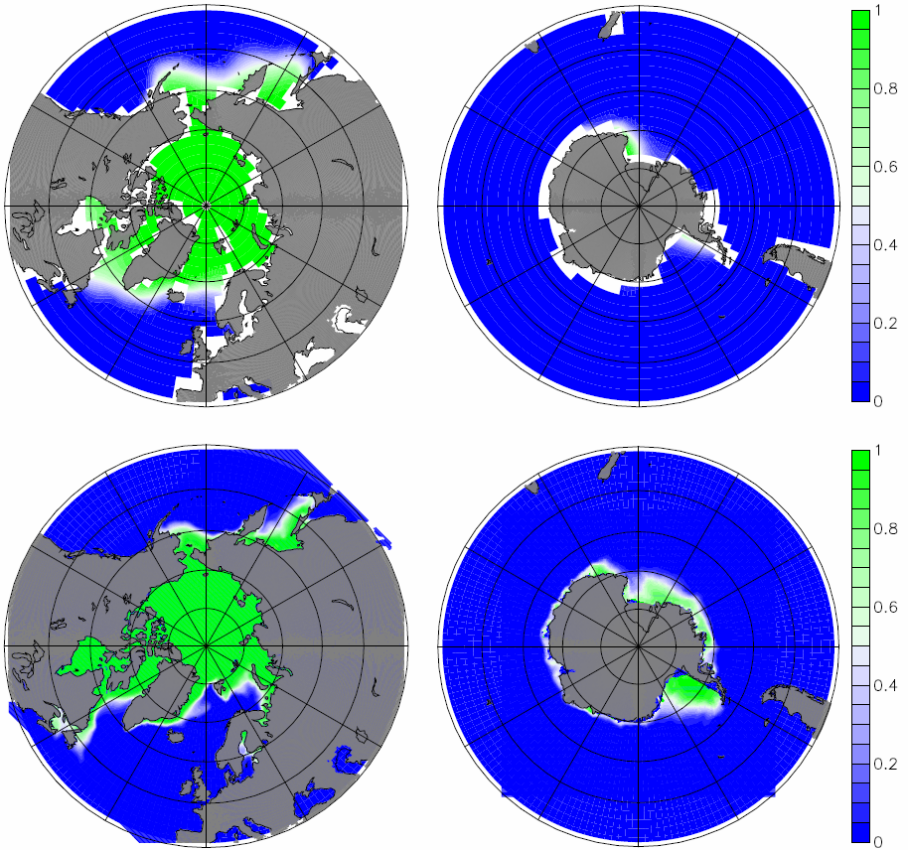

Fig. 7. The sea ice cover fraction in March in the Arctic (left) and the Antarctic (right). The top row shows the SPEEDO ensemble mean and bottom row the data from Cosimo (2008).

GMDD

2, 1115–1155, 2009

Efficient primitive equation climate model SPEEDO

C. A. Severijns and W. Hazeleger

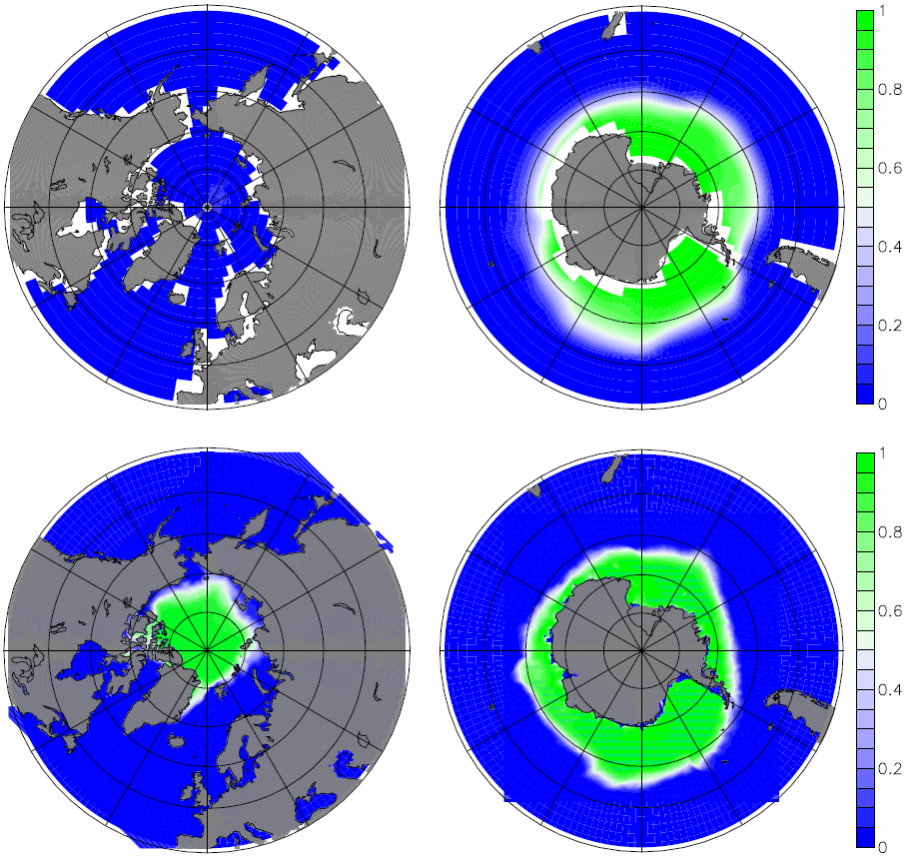

Fig. 8. Same as Fig. 7 but for September.

GMDD
2, 1115–1155, 2009

Efficient primitive equation climate model SPEEDO

C. A. Severijns and W. Hazeleger

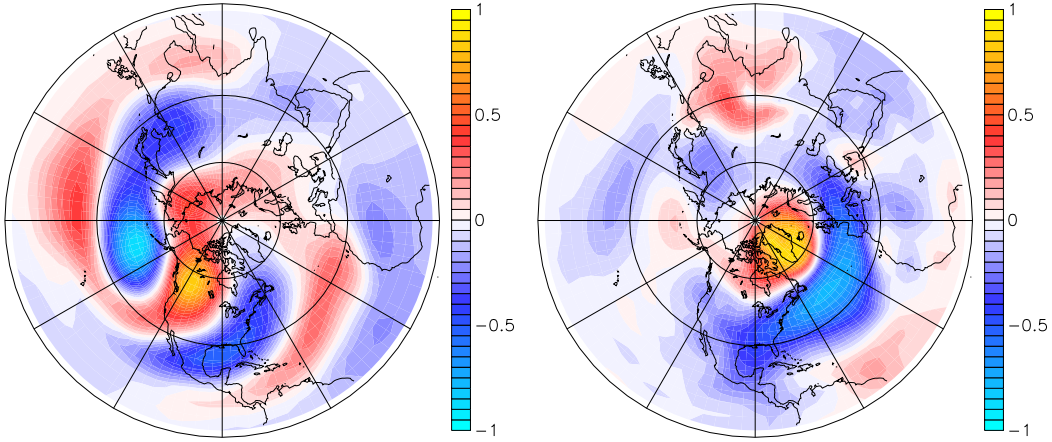

Fig. 9. The correlation of the geopotential height anomalies at 500 hPa with the PNA index (left) and the correlation of the mean sea-level pressure anomalies with the NAO index (right).

GMDD

2, 1115–1155, 2009

Efficient primitive equation climate model SPEEDO

C. A. Severijns and W. Hazeleger

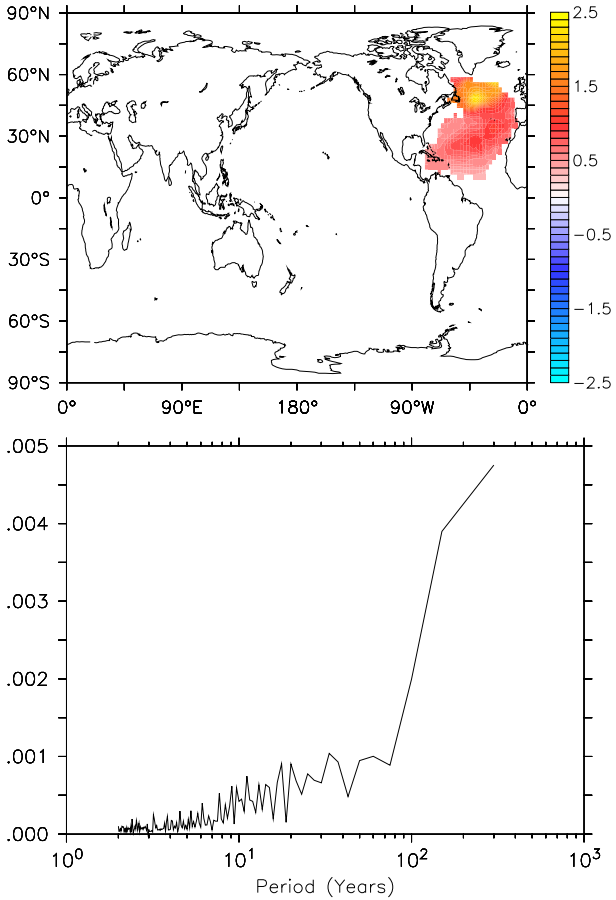

Fig. 10. The regression of the SST with the AMO index in $10^{-6}\,\mathrm{K\,s\,m^{-3}}$ (top) and the power spectrum of the AMO index time series in K^2 (bottom).

GMDD

2, 1115–1155, 2009

Efficient primitive equation climate model SPEEDO

C. A. Severijns and W. Hazeleger

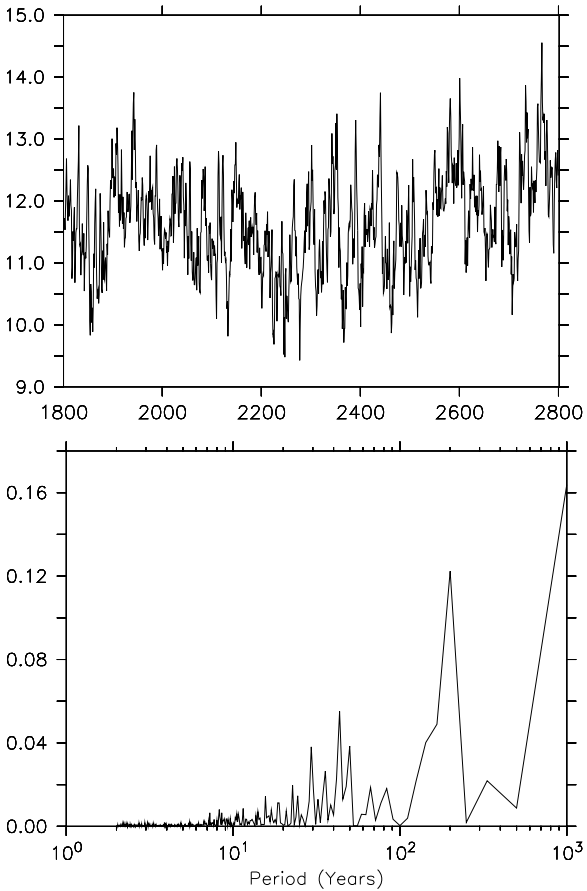

Fig. 11. The annual mean of the monthly maximum strength of the AMOC in the North Atlantic in $10^6\,m^3\,s^{-1}$ in the control run (top) and the power spectrum of this time series in $10^{12}\,m^6\,s^{-2}$ (bottom).

GMDD

2, 1115–1155, 2009

Efficient primitive equation climate model SPEEDO

C. A. Severijns and W. Hazeleger

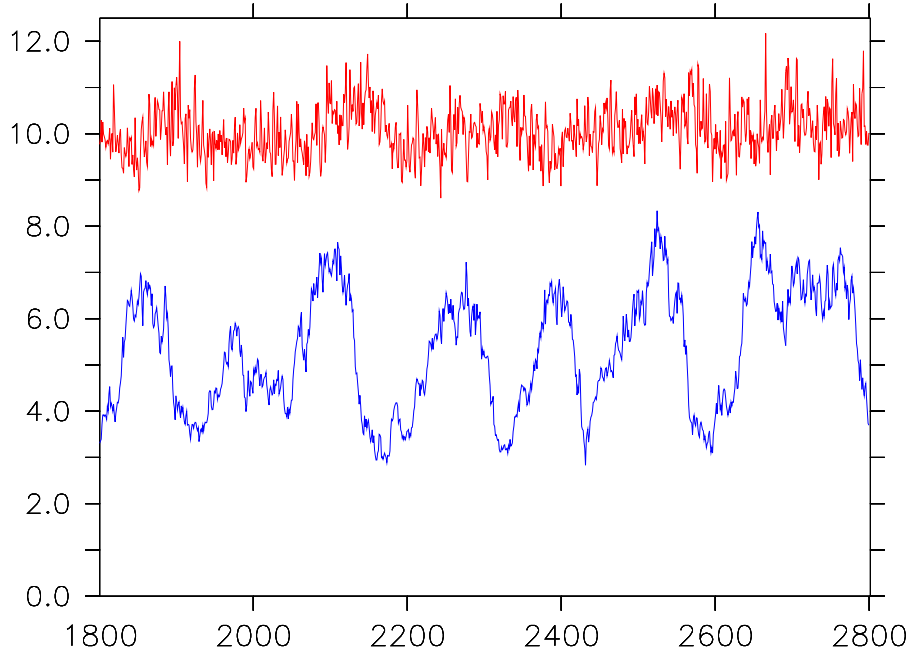

Fig. 12. The annual mean Arctic (red) and Antarctic (blue) sea ice volume in 10^{12} m^3 during the 1000 year control run.

GMDD

2, 1115–1155, 2009

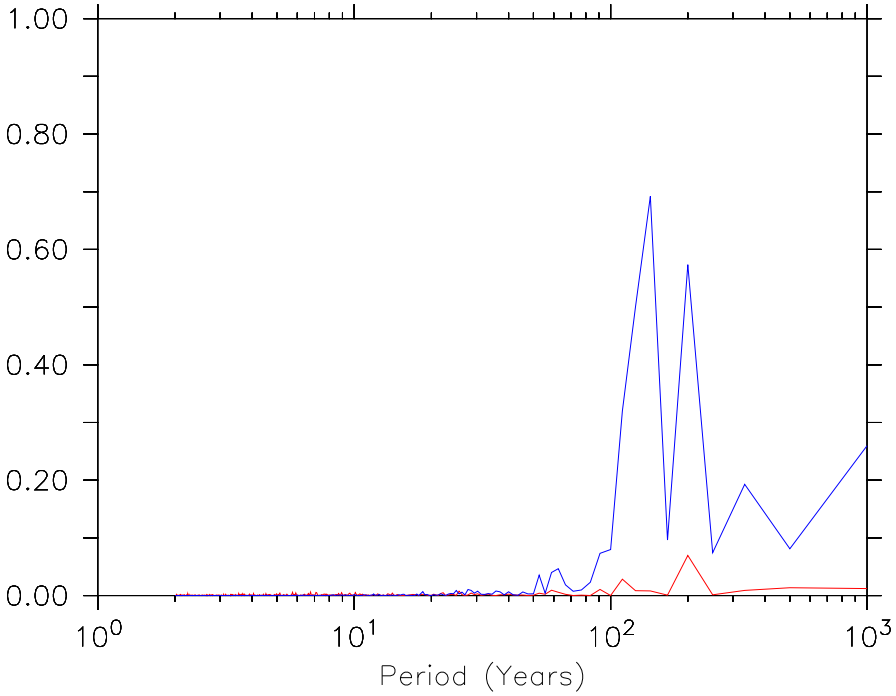

Fig. 13. The power spectra of the Arctic (red) and Antarctic (blue) sea ice volume in 10^{24} m^6 in the control run.

GMDD

2, 1115–1155, 2009

Efficient primitive equation climate model SPEEDO

C. A. Severijns and W. Hazeleger

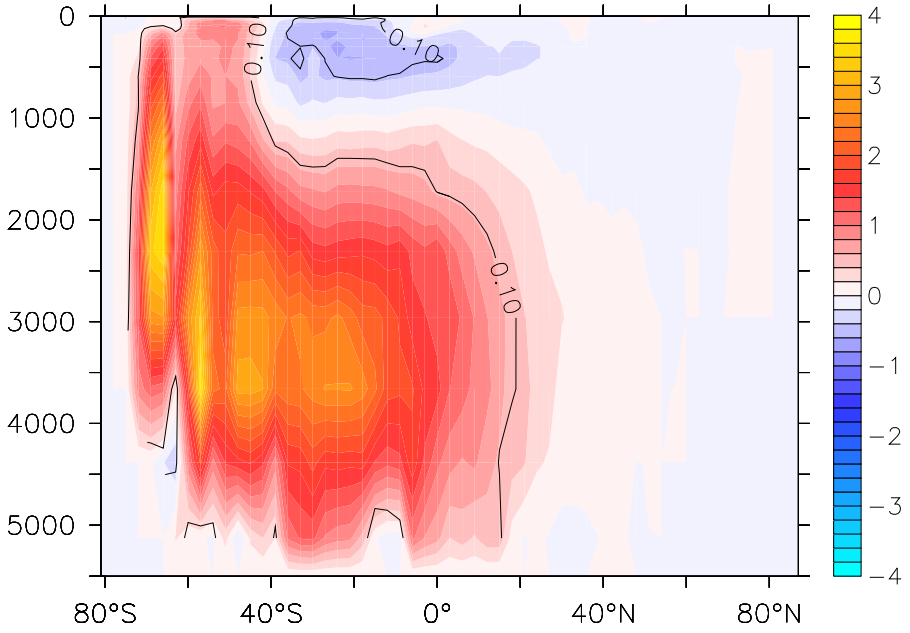

Fig. 14. The regression of the Antarctic sea ice volume with the strength of the global meridional overturning circulation in $10^{-6}\,s^{-1}$. The contour indicates the area where the regression coefficient is statistically significant.

GMDD
2, 1115–1155, 2009

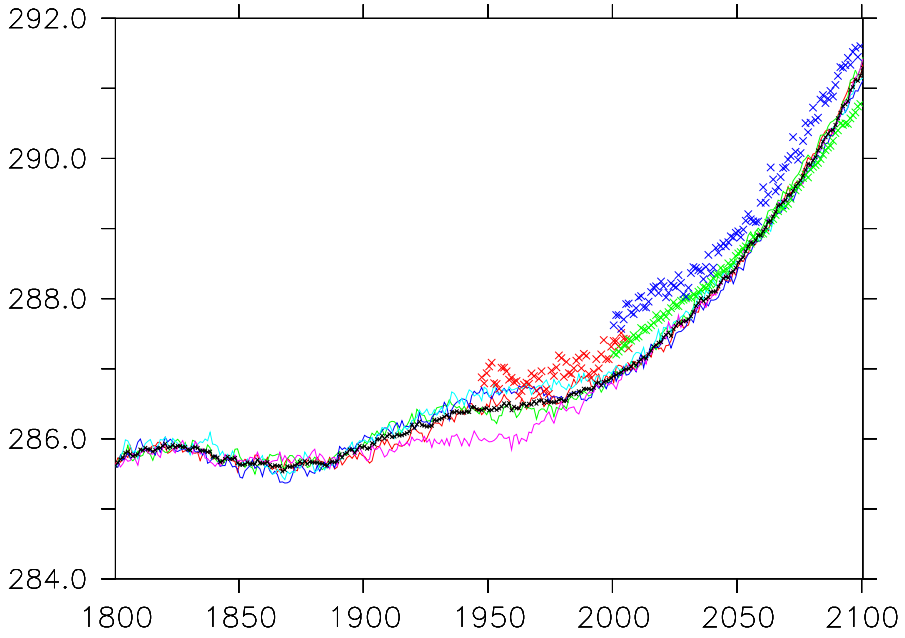

Fig. 15. The annual global mean two meter temperature in K from 1800 to 2100 in each of the SPEEDO ensemble members (thin red, green, light blue, blue and purple lines) and the ensemble mean (thick black line). Also shown are the reanalysis data from 1950 to 2008 (red crosses) and the ensemble mean two meter temperature of the five ECHAM5-MPI/OM CMIP3 simulations (green crosses) and of the three NCAR CCSM3 CMIP3 runs (blue crosses) from 2000 to 2100.

GMDD
2, 1115–1155, 2009

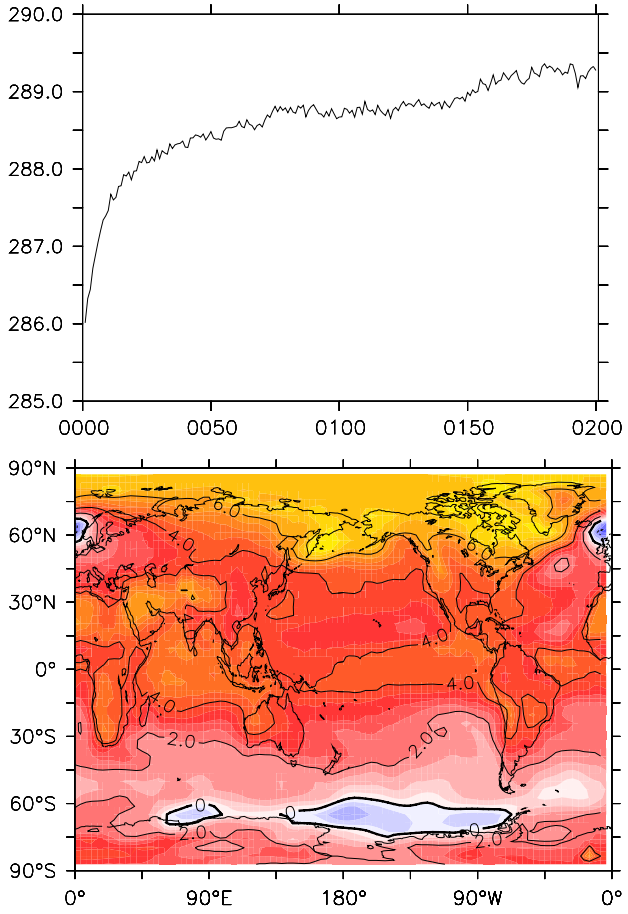

Fig. 16. The time series of the annual mean two meter temperature in K (top) and the difference in the 100 year mean two meter temperature of the $2\times CO_2$ experiment and the control run in K in the second 100 years (bottom).

GMDD

2, 1115–1155, 2009

Efficient primitive equation climate model SPEEDO

C. A. Severijns and W. Hazeleger

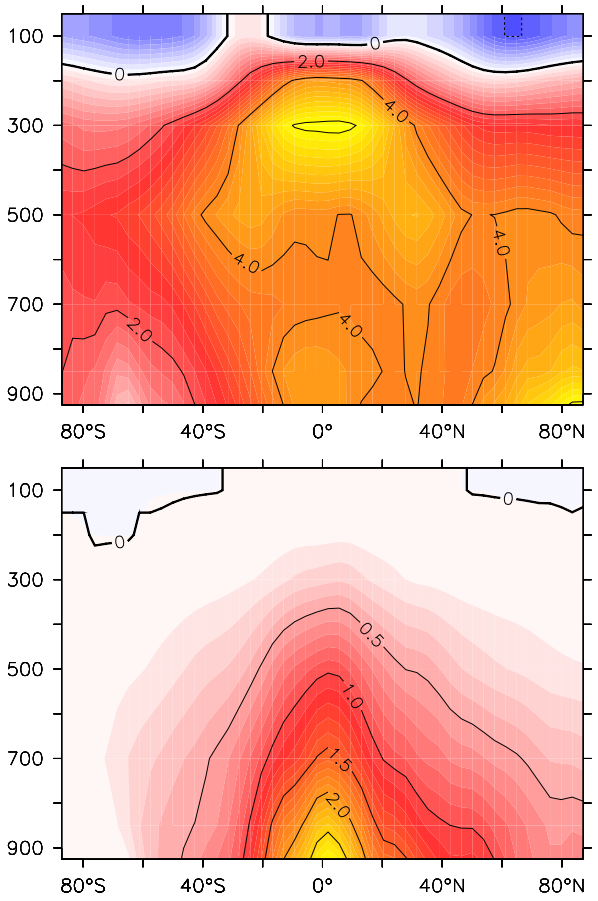

Fig. 17. The difference of the zonal mean temperature in K (top) and zonal mean specific humidity in 10^{-3} kg kg^{-1} (bottom) of the $2\times CO_2$ experiment and the control run.

GMDD
2, 1115–1155, 2009

Efficient primitive equation climate model SPEEDO

C. A. Severijns and W. Hazeleger

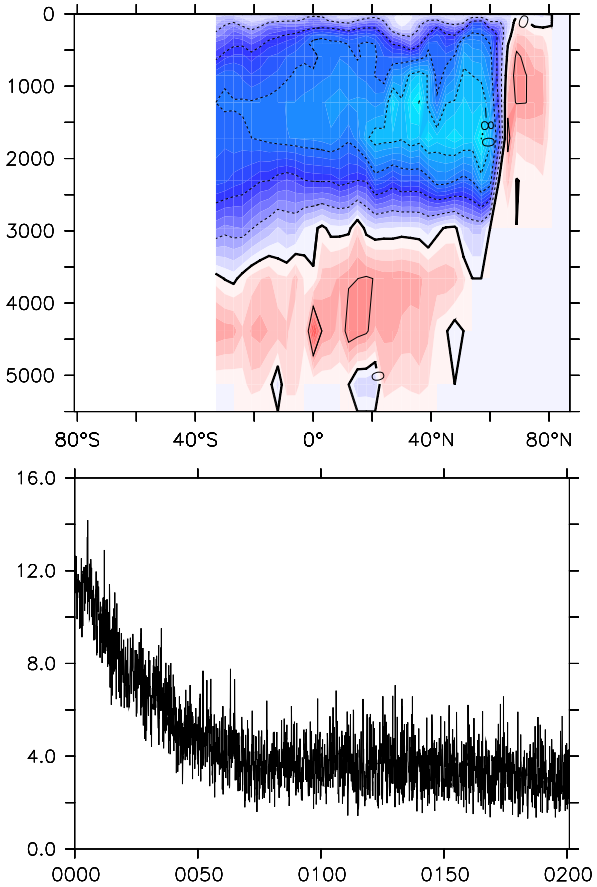

Fig. 18. The difference in the Atlantic meridional overturning stream function between the $2\times CO_2$ experiment and the control run (top) and the time series of the maximum AMOC strength in the $2\times CO_2$ experiment (bottom), both in $10^6\,m^3\,s^{-1}$.

GMDD
2, 1115–1155, 2009

Efficient primitive equation climate model SPEEDO

C. A. Severijns and W. Hazeleger

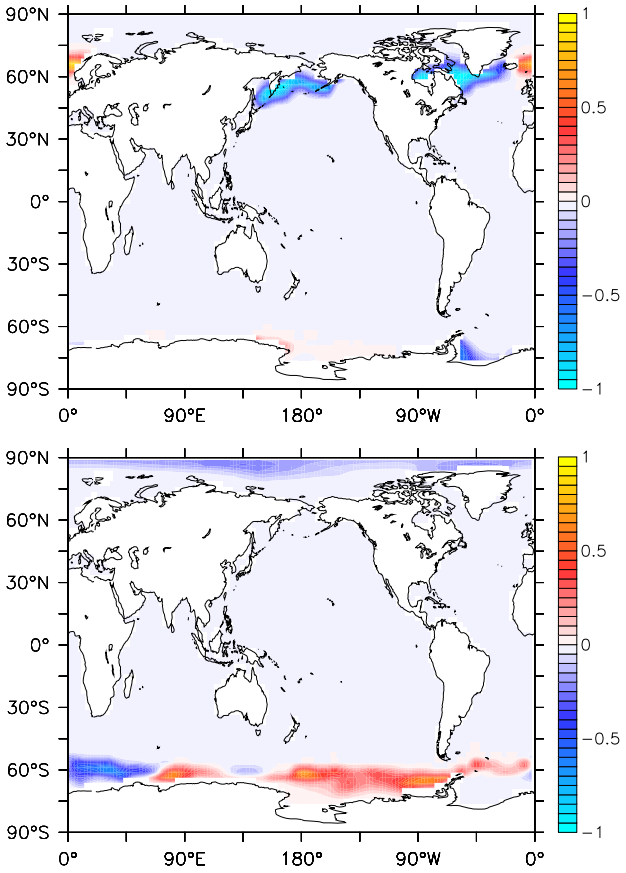

Fig. 19. The change in the sea ice cover in March (top) and September (bottom) of the $2\times CO_2$ experiment and the control run.

GMDD
2, 1115–1155, 2009

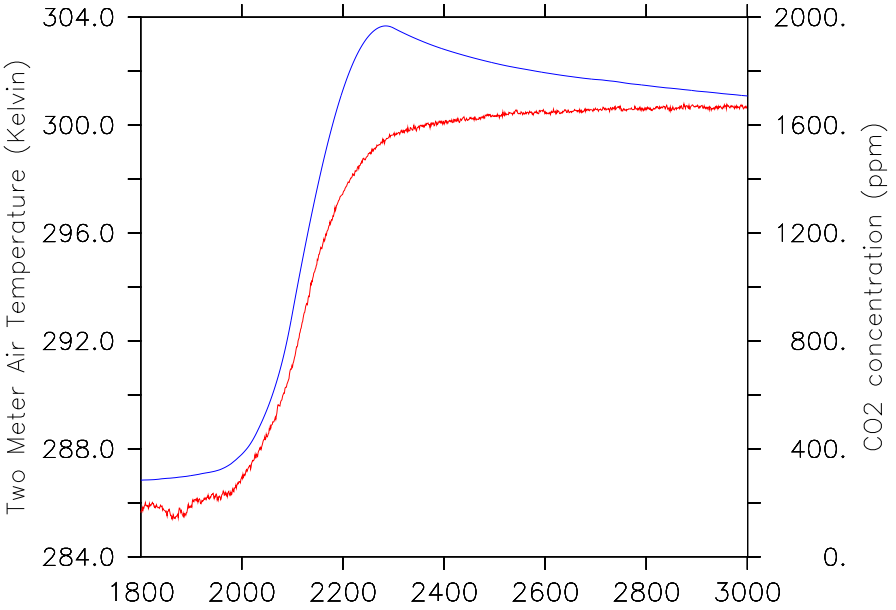

Fig. 20. The annual global mean two meter air temperature in K (red) and prescribed CO_2 concentration (blue) in ppm in the scenario run.

GMDD

2, 1115–1155, 2009

Efficient primitive equation climate model SPEEDO

C. A. Severijns and W. Hazeleger

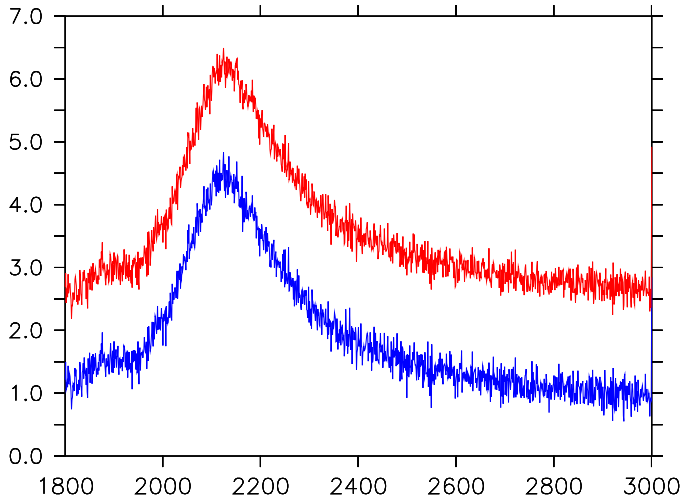

Fig. 21. The annual global mean TOA net radiation budget (red) and surface heat budget (blue) in W m^{-2} in the scenario run.

GMDD

2, 1115–1155, 2009